Insight into silicate-glass corrosion mechanisms

CÉLINE CAILLETEAU[1], FRÉDÉRIC ANGELI[1], FRANÇOIS DEVREUX[2]*, STÉPHANE GIN[1], JACQUES JESTIN[3], PATRICK JOLLIVET[1] AND OLIVIER SPALLA[4]

[1]CEA, DEN, Laboratoire d'étude du Comportement à Long Terme, 30207 Bagnols-sur-Cèze, France
[2]Laboratoire de Physique de la Matière Condensée, Ecole Polytechnique-CNRS, 91128 Palaiseau, France
[3]Laboratoire Léon Brillouin, CNRS-CEA, 91191 Gif-sur-Yvette, France
[4]CEA, DSM, Laboratoire Interdisciplinaire sur l'Organisation Nanométrique et Supramoléculaire, 91191 Gif-sur-Yvette, France
*e-mail: francois.devreux@polytechnique.fr

Published online: 26 October 2008; doi:10.1038/nmat2301

The remarkable chemical durability of silicate glass makes it suitable for a wide range of applications. The slowdown of the aqueous glass corrosion kinetics that is frequently observed at long time is generally attributed to chemical affinity effects (saturation of the solution with respect to silica). Here, we demonstrate a new mechanism and highlight the impact of morphological transformations in the alteration layer on the leaching kinetics. A direct correlation between structure and reactivity is revealed by coupling the results of several structure-sensitive experiments with numerical simulations at mesoscopic scale. The sharp drop in the corrosion rate is shown to arise from densification of the outer layers of the alteration film, leading to pore closure. The presence of insoluble elements in the glass can inhibit the film restructuring responsible for this effect. This mechanism may be more broadly applicable to silicate minerals.

Silicate minerals and glasses are not only naturally abundant on the earth's surface but are also fundamental components of innumerable manufactured materials including glass, ceramics, gels, monocrystals and cement. The mechanisms occurring on the surface of silicate materials have been investigated in the earth sciences to model element mass balances in the earth's crust during their geochemical cycle[1–3], as well as in technological applications to enhance the durability of industrial glass products[4–6]. Interactions with water are particularly important[7–9], especially for glass used as a containment matrix for radionuclides arising from spent-nuclear-fuel treatment[10–12]. Their lifetime must exceed several tens of thousands of years to guarantee the safety of a geological repository. Although the behaviour of such materials can be estimated over very long periods by examining natural or archaeological analogues[13,14], it is indispensable to have a deep understanding of the key mechanisms to improve the robustness and the reliability of the predictive models.

The corrosion of silicates arises from several coupled mechanisms: hydration, hydrolysis of the ionic–covalent network and exchange between alkali or alkaline-earth ions and protons in solution[15,16]. Depending on the materials and the leaching conditions, various secondary phases may precipitate from dissolved elements[17–19]. In most cases, an amorphous film forms on the surface of the mineral or glasses, whose structure can be modified by *in situ* repolymerization of the silica network following the release of soluble elements[15,16,20,21]. This amorphous, porous, hydrated layer is commonly referred to as a 'gel'. Its thickness varies significantly—from a few nanometres to macroscopic size—with the glass or mineral composition and with the leaching time and conditions. Its effect on the alteration kinetics is a debated question[19]. Some authors claim that it constitutes a barrier with respect to the diffusion of reactive species between the pristine material and solution[22–26]. Others deny this role and attribute the experimentally observed drop in the corrosion rate only to the solution saturation and inhibiting effects[27–29]. To resolve this issue we must first identify the structural and morphological transformations occurring within the alteration film, then determine the manner in which they modify transfers between the pristine material and solution and affect the material durability.

The impact of the gel structural transformations on the diminishing corrosion rate was demonstrated directly by coupling several experimental techniques (gas adsorption isotherm, X-ray and neutron scattering, mass spectroscopy and electron microscopy) and numerical simulations at mesoscopic scale by a Monte Carlo method. Six glass compositions were investigated: $(61-x)SiO_2{\cdot}xZrO_2{\cdot}17B_2O_3{\cdot}18Na_2O{\cdot}4CaO$, where x ranged from 0 to 8 mol%. These glass compositions are hereafter designated xZr. The composition was selected to approximate the proportions of the major oxides (with the exception of Al_2O_3) of the French reference nuclear glass[30]. The actual glass contains only 2% zirconia, but here it is a surrogate for all the insoluble oxides, including those of most radionuclides. Substituting zirconia partially for a fraction of the silica enabled us to characterize the influence of insoluble oxides on the alteration kinetics and on the morphology of the altered layer. Moreover, these compositions comprise the three broad categories of oxides found in the glass: network formers (Si, Zr, B), network modifiers or charge compensators (Na, Ca). Leaching experiments were carried out on calibrated powders at 90 °C with a solution buffered to pH 6.9 ± 0.1; buffering the solution mitigated the effect of pH variations that would otherwise have modified the alteration conditions when certain ions (Na^+, $B(OH)_3$, $H_4BO_4^-$) were released into solution. Two types of experiment were carried out to measure

Table 1 Initial dissolution rate r_0 and silica concentration at saturation C_{Si} versus ZrO_2 content x (90 °C at pH 6.9).

x (%)	0	1	2	4	6	8
r_0 (g m^{-2} d^{-1})	37	15	5.1	1.30	0.19	0.091
C_{Si} (mg l^{-1})	133	141	140	118	100	87

the initial dissolution rate and to characterize alteration under silica saturation conditions (refer to the Methods section). Table 1 shows that the initial dissolution rate, controlled by hydrolysis of the silicate network, dropped very significantly as the zirconia content increased in the glass, with only a relatively slight reduction in the silicon concentration at saturation. The concentrations of about 140 mg l^{-1} obtained for the glasses with low zirconia content correspond to the solubility of amorphous silica at the experimental temperature and pH. The dissolved boron fraction is plotted versus time for the test glasses in Fig. 1. As boron is fully soluble under these experimental conditions, the dissolved boron fraction is an indicator of the degree of glass corrosion[31]. A major drop in the corrosion rate was observed after increasing time intervals and at increasingly high levels for the glass samples containing 0, 1 and 2% ZrO_2. Conversely, corrosion continued after saturation of the solution with respect to silica, and was practically complete for the glasses with 4, 6 and 8% ZrO_2. In these compositions zirconium is found at coordination number 6, inserted in the silicate network by Si–O–Zr bonds[32]; it conserves a similar local structural environment in the gel[33]. Our results show that substituting zirconium for silica considerably slows the glass dissolution kinetics, but ultimately leads to a much greater degree of corrosion. To account for these results the morphology of the alteration film was characterized by various techniques and simulated by a Monte Carlo method to obtain topological data on the evolution of the porous network, especially with regard to open or closed porosity.

A first approach was to observe the penetration of dye molecules into the gel. Altered glass monoliths were immersed for one hour in 10 ml of leaching solution containing 10^{-3} M methylene blue, then washed and dried. Their colouring provided a qualitative indication of the dye penetration into the gel pores. The photographic insets in Fig. 2 show that the sample without zirconia (0Zr) was highly coloured after 8 h of leaching (before corrosion was inhibited) but only slightly after two months of leaching alteration (after inhibition). Conversely, sample 8Zr remained coloured even at the end of the leaching period. Time-of-flight/secondary-ion mass spectroscopy (ToF-SIMS) provided a more quantitative evaluation of the dye penetration. This technique consists in sputtering the sample surface layer by layer and analysing the elemental concentration profiles by mass spectrometry. Sulphur was used as a marker for methylene blue. The results for sample 0Zr leached for 8 h and for two months are shown in Fig. 2. It is immediately apparent that the altered zone no longer contained any B, Na or Ca and that the total gel thickness was slightly smaller at the end of leaching than after 8 h. The latter point might seem surprising, because the final alteration degree was about twice the value obtained after 8 h (Fig. 1), but this apparent contradiction can be explained by partial gel dissolution and by densification of the gel resulting in its shrinkage (see below). The dye penetrated into the outer part of the gel at the beginning of leaching, but practically no longer at the end of the process. This confirms the visual observation and gives a first indication that the initially open porosity progressively closed as the gel developed. However, this is not fully conclusive, because the size of the dye molecules may prevent them from entering the smallest pores.

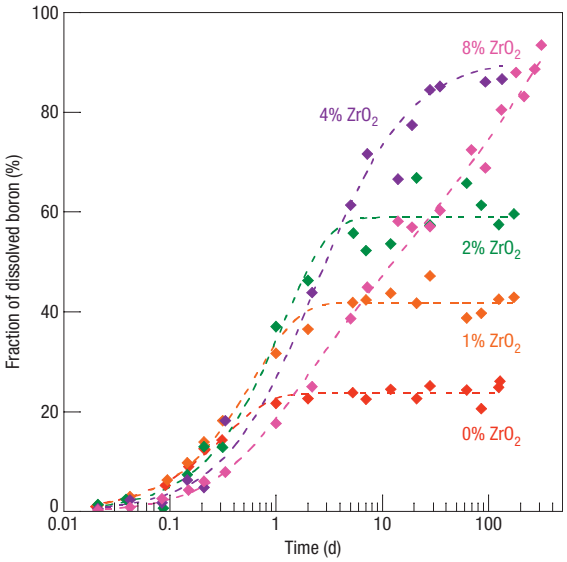

Figure 1 Glass alteration kinetics. Dissolved boron fraction versus time for glass samples 0Zr, 1Zr, 2Zr, 4Zr and 8Zr. The kinetics for sample 6Zr (not shown) were comparable to those of 8Zr, but more rapid. Dashed lines are visual guidelines. The data accuracy is ±2.5%.

Another method consists in comparing the specific surface areas measured by small-angle X-ray scattering (SAXS) and by gas adsorption. These two techniques should give different results in the event of closed porosity, as the entire porous structure scatters X-rays, whereas gas adsorption is possible only in pores open to the bulk solution. The gel morphology after different leaching times was systematically investigated by SAXS. The evolution of the X-ray scattering curves indicates a structural reorganization of the gel during leaching (Fig. 3). The elementary mechanisms responsible for the reorganization are the hydrolysis of the siloxane bonds and the condensation of the silanol moieties[15,16]. The initially filamentary structures became increasingly branched and the pore size increased. The reorganization was sufficient in glass 0Zr to reach at the longest leaching time the so-called Porod regime, where the scattering is controlled by the smooth surface of the pores[34]. The Porod regime is characterized by a scattered intensity that varies as $\Sigma^* q^{-4}$, where Σ is the specific surface area and q the scattering-vector modulus (Fig. 3a). The measured surface area was 84 ± 4 m^2 g^{-1} after 39 days of leaching and 63 ± 3 m^2 g^{-1} after 125 days, indicating that the gel continued to undergo structural reorganization well after the rate drop. By comparison, the surface area determined from the krypton adsorption isotherm using the Brunauer–Emmett–Teller model[35] was only 2.2 ± 0.3 m^2 g^{-1} after 125 days of leaching. As the gas adsorption experiment required previous outgassing by vacuum heat treatment that could have caused the gel porosity to collapse, we verified that the specific surface area measured by SAXS remained unchanged after this treatment. The difference between the surface areas measured by these two techniques is another indication of porosity closure in the glass without zirconia. The restructuring occurred much more slowly in the other glasses, for which the SAXS specific surface area cannot be determined, because the pores were neither large nor smooth enough to reach the q^{-4} Porod regime (Fig. 3b).

A much more powerful technique for characterizing closed porosity is neutron scattering with index matching[36]. The leaching solution (100% H_2O) is replaced by a mixture of H_2O and D_2O with the same neutron scattering cross-section as the gel material.

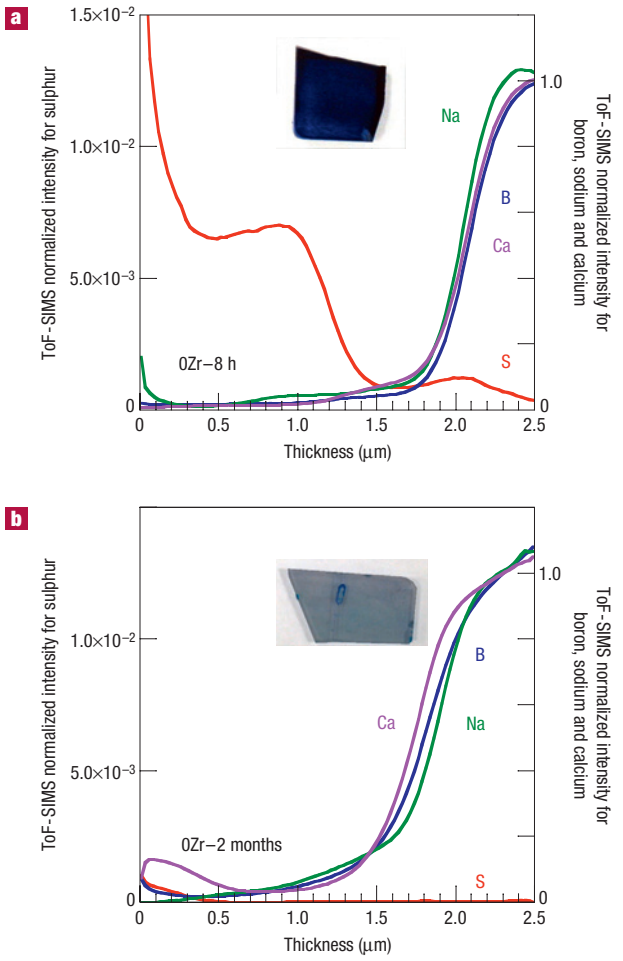

Figure 2 Dye penetration into the gel in sample 0Zr. a,**b**, ToF-SIMS concentration profiles for B, Na, Ca and S normalized to silicon after 8 h (**a**) and 2 months (**b**) of leaching. Sulphur was used as a tracer for methylene blue. The photographic insets show the dye-impregnated monoliths.

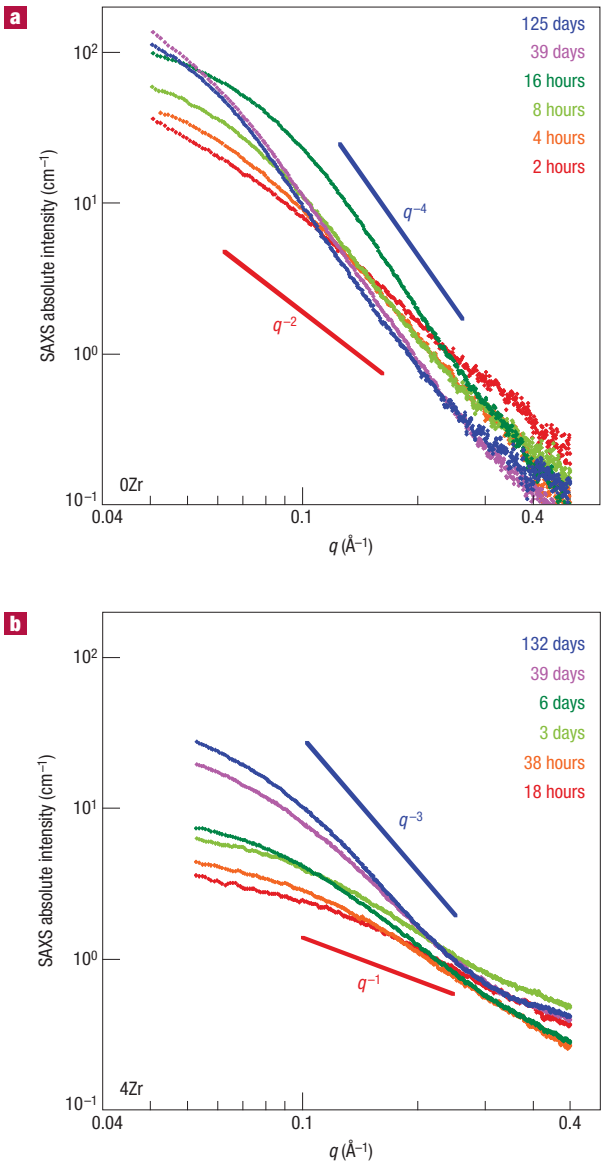

Figure 3 Small-angle X-ray scattering. a,**b** Scattered intensity versus scattering-vector modulus (q) after different alteration times for samples 0Zr (**a**) and 4Zr (**b**). The variations approximating to q^{-1} or q^{-2} observed for short durations are characteristic of scattering by linear or ramified structure, respectively. The q^{-4} behaviour observed for glass 0Zr for the longest durations indicates scattering by smooth pores of sufficient size.

Under these conditions the contrast disappears when the mixture enters the open pores, but persists if closed porosity prevents any exchange. To prevent solvent exchange from initiating renewed alteration and modifying the gel, the H_2O–D_2O mixture was prepared from solutions obtained by previous leaching under the same conditions and for the same time as the test gel. Figure 4 shows scattering curves for H_2O, D_2O and several mixtures near the index-matching value for sample 0Zr at the beginning and end of alteration and for sample 4Zr at the end of alteration. The stronger signal observed for small q is due to scattering by the grain envelopes, whereas the porous structure is responsible for scattering at the intermediate range of q (0.01–0.1 Å^{-1}). Solvent exchange resulted in extinction of the scattering signal between 0.01 and 0.1 Å^{-1} with mixtures near 30% H_2O and 70% D_2O for sample 0Zr at the beginning of alteration and for sample 4Zr at the end of alteration, but not for sample 0Zr at the end of alteration. This clearly proves that the restructuring of the gel layer leads to the closure of the pores in the glass without zirconia, whereas this transformation is inhibited in the 4% ZrO_2 glass.

Finally, Fig. 5 shows scanning transmission electron microscopy images of sample 0Zr after leaching. The 100-nm-thick gel slice has been obtained by focused-ion-beam milling. The total gel thickness is 3–4 μm (Fig. 5a). A non-porous gel region 150 nm thick is clearly visible near the outer edge (Fig. 5b). The presence of this dense layer explains fairly well the pore closure demonstrated by the three experiments described above. The gel porosity is revealed by the granularity of the image with pore sizes ranging from 2 to 20 nm (Fig. 5c). Scanning transmission electron microscopy images revealed an increase of the mean pore size from the glass–gel edge towards the dense zone, indicating a more important pore ripening in the most aged zones of the gel. Moreover, an analysis of the electron energy losses shows that the boron concentration gently decreases from the glass–gel interface in sample 0Zr (over about 250 nm), whereas it shows a sharp transition to zero in sample

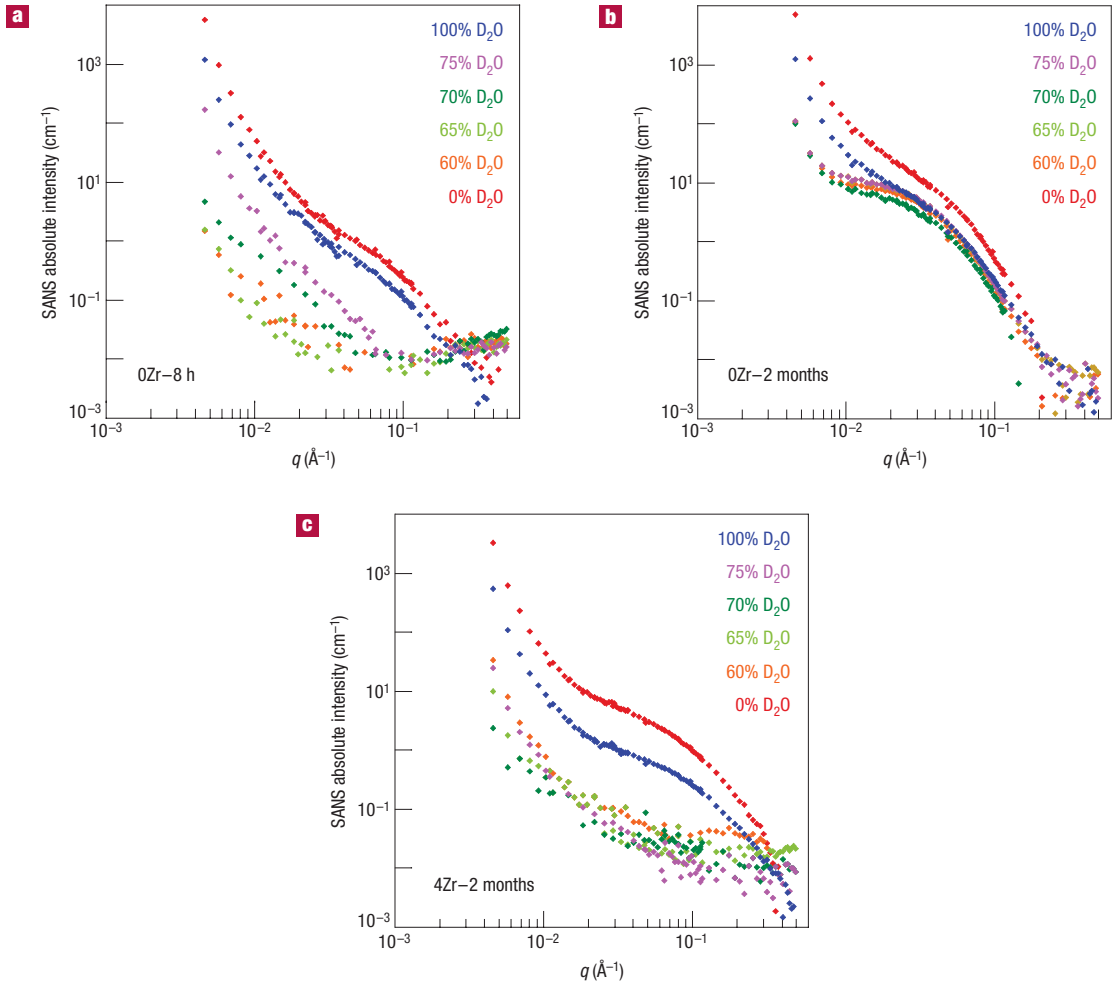

Figure 4 Neutron scattering with contrast variation. a–c, Scattered intensity versus scattering-vector modulus with different solution isotopic compositions for sample 0Zr after leaching for 8 h (**a**) and 2 months (**b**), and for sample 4Zr at the end of alteration (**c**). The resulting flat level of the scattering intensity at the high q values is of the order of magnitude of the experimental background.

8Zr (Supplementary Information, Fig. S1). This suggests that the porosity closure in sample 0Zr limits the transport of mobile species within the gel.

To interpret these results we developed a Monte Carlo simulation model of multi-element glass alteration[37]. In this model the network-forming cations (Si, B) are randomly distributed at the nodes of a diamond lattice, the cations at coordination number 6 (Zr) are placed inside a cage of six SiO_4 tetrahedrons and the alkali or alkaline-earth ions at interstitial positions either as charge compensators (B^{IV}, Zr^{VI}) or as network modifiers generating non-bridging oxygen atoms. Considering a regular lattice enables us to take into account a very large number of atoms (about 100 million) without significantly affecting the mechanisms involved, which are based on the comparable short-range order of vitreous and crystalline systems. Dissolution kinetics are characterized by dissolution probabilities that depend on the nature of the cation and its environment. The release of soluble elements generates a porous structure that reorganizes driven by the dynamics of hydrolysis and recondensation of the silicate bonds. In the absence of any oxides less soluble than silica, this structural reorganization leads to increased pore size and smoothness that is consistent with X-ray scattering experiments (Fig. 3). Densification of the outer gel layers is also observed together with pore closure and significant shrinkage. The morphology arising from this process is shown in Fig. 6. It shows the same characteristics as the electron microscope image: the presence of closed porosity and a densified outer gel layer. This structural change prevents the release of soluble elements and inhibits further corrosion. This model quantitatively reproduces the effect of the concentration of soluble elements (boron and alkali ions) on the alteration kinetics[38]. The addition of oxides less soluble than silica slows the leaching kinetics, but also hinders the gel structural reorganization. As a result the pores remain small and rough; densification and shrinkage are no longer observed. The porosity closes only intermittently, resulting in continued alteration. The presence of very insoluble elements thus paradoxically leads to a greater degree of corrosion that is consistent with the experimental results shown in Fig. 1.

A cause–effect relationship between the altered layer morphology and the leaching kinetics has been established using complementary experimental techniques. Substituting an insoluble oxide (zirconia in this case) for a significant fraction of silica prevents the gel structural reorganization and, by inhibiting the pore closure mechanism, leads to a greater corrosion. The large drop in the leaching rate observed for some glass compositions

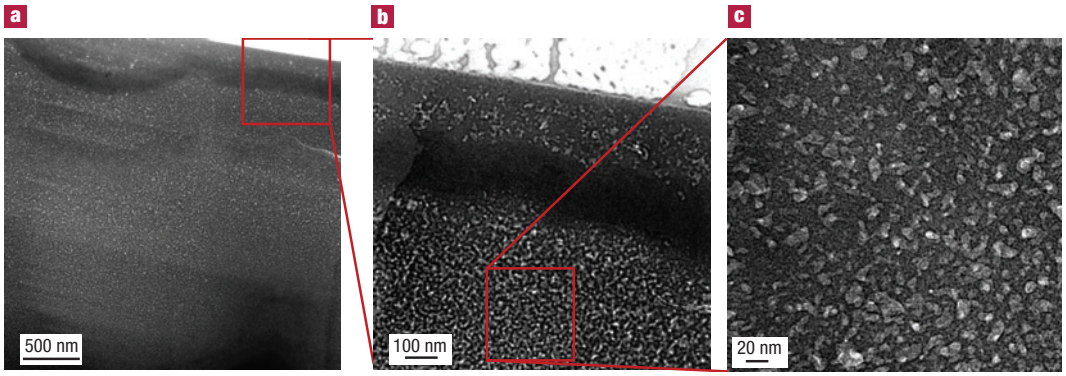

Figure 5 Scanning transmission electron microscopy of sample 0Zr at the end of alteration. a, The gel (top) is slightly lighter than the pristine glass (bottom); **b**, detail of the dark band corresponding to the densified zone of the outer gel layers; **c**, magnification of the pores.

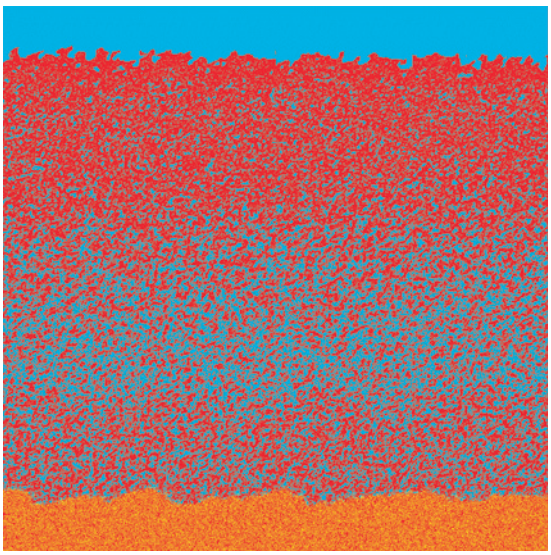

Figure 6 Monte Carlo simulation of the gel layer. A longitudinal cross-section of the gel obtained by simulation of the alteration of a glass with the same composition as 0Zr. The silicon atoms are shown in red, other elements in yellow. Water in blue.

is due to pore closure by gel densification, which transforms the glass from a state in which corrosion is controlled mainly by hydrolysis to a state in which it is controlled by the accessibility of the reaction interface to water. These findings point out that this mechanism has to be considered to investigate the alteration-rate-drop regime; the thermodynamic saturation calculated from experimental measurements of the Gibbs free energy of formation of sodium borosilicate glass showed that neither a global affinity[39] nor a first-order rate law on the basis of the silica alone[40] were able to account for the experimental rate drop[41]. The approach to the steady state is an intricate process that results from complex exchanges between the solution and the dynamically reorganizing heterogeneous gel structure. Under these conditions, it is unlikely that it can be simply described by an affinity law on the basis of a single (even if complicated) chemical equilibrium. The saturation of the solution with respect to silica is a prerequisite to the formation of a passivating layer but is not a criterion for the end of corrosion[42]. Regardless of the degree of reaction progress, even under 'saturation' conditions, aqueous alteration of nuclear glasses continues to release glass constituent elements, even if only at extremely low values[43]. The alteration film constitutes a diffusion barrier with (in the case of the French nuclear glass[43,44]) an apparent diffusion coefficient of about 10^{-21}–10^{-24} $m^2\,s^{-1}$, very near the values found in solids. Such very low values could not be reached if the porosity were open, enabling percolation of the elements released from the glass into solution because the interdiffusion coefficients (for transfer by direct contact between the pristine glass and solution) are much higher[16,45].

Although the pore-closure mechanism identified here concerns borosilicate glasses, it could be extended to the dissolution of other natural or manufactured glasses or more broadly to silicate minerals on the basis of similarities in their macroscopic behaviour and certain microscopic features: morphological similarities have been observed with the alteration layer on basaltic glasses or feldspars with the presence of a porous, amorphous and hydrated interphase arising from local silica hydrolysis and condensation reactions[14,46,47]. We may postulate the hypothesis that an alteration layer consisting mainly of silica, if sufficiently restructured, could limit the accessibility of the reaction interface to the reactive species. Conventional kinetic laws on the basis only of chemical thermodynamics[48–50] cannot fully describe the alteration kinetics, especially over extended timescales. Structural transformations in the surface layer must then be taken into account, together with coupling between chemical reactions and species transport in the layer. The evolution of the porosity and its possible closure should be considered as a basic mechanism that can be affected by the environment in which the material is found. For example, the presence of crystallized secondary phases can consume elements in the gel and thereby inhibit its structural reorganization. All these phenomena must be considered to develop mechanistic models for predicting the alteration of glass and silicate minerals.

METHODS

Glass samples were prepared by melting a mixture of SiO_2, ZrO_2, H_3BO_3, Na_2CO_3 and CaO at 1,300 °C. After quenching at room temperature in graphite crucibles measuring 2.5 cm × 2.5 cm, the samples were annealed for 1 hour at 600 °C. The glass compositions were analysed by inductively coupled plasma atomic emission spectroscopy. Monoliths 3 mm thick were cut from the glass blocks and polished to obtain a surface roughness of less than 1 μm. Calibrated powder samples were obtained by pulverizing the glass blocks and sieving the powder; the specific surface area measured by krypton adsorption according to the Brunauer–Emmett–Teller method was $1{,}500 \pm 200\,cm^2\,g^{-1}$ for the 20–40 μm fraction and $500 \pm 30\,cm^2\,g^{-1}$ for the 80–125 μm fraction. The initial

dissolution rates were measured with a glass-surface-area-to-solution-volume (SA/V) ratio of $10\,m^{-1}$ (90 mg of powder from the 80–125 μm fraction in 450 ml of solution). The overall leaching kinetics were measured with an SA/V ratio of $1{,}500\,m^{-1}$ (4 g of powder from the 20–40 μm fraction in 400 ml of solution). The monoliths used for ToF-SIMS and transmission electron microscopy experiments were leached together with powder to ensure the same SA/V as for the kinetics. The concentrations in solution were measured by colorimetry (Si, Ca) and by capillary electrophoresis (B, Na) and verified at the end of the experiment by inductively coupled plasma atomic emission spectroscopy (Si, Zr, B, Na, Ca). ToF-SIMS profiles were obtained with a spectrometer using oxygen for abrasion and bismuth for analysis. The measured intensities for isotopes ^{11}B, ^{23}Na and ^{40}Ca were normalized with respect to ^{30}Si, then divided by the corresponding mean value in the unaltered glass using the following relation:

$$S_X = \frac{(I_X/I_{Si})_{\text{alteration layer}}}{(I_X/I_{Si})_{\text{pristine glass}}},$$

where I_X and S_X are the raw and normalized intensities of element X ($X = {}^{11}B$, ^{23}Na, ^{40}Ca) and I_{Si} the raw intensity of isotope ^{30}Si. S_X thus quantifies the excess or deficit of element X with respect to its concentration in the pristine glass. The sulphur intensity was normalized only with respect to silicon-30. Neutron scattering experiments were carried out with the PACE diffractometer in the Leon Brillouin Laboratory (Saclay, France) and X-ray scattering experiments with a laboratory-built diffractometer.

Received 18 July 2008; accepted 24 September 2008; published 26 October 2008.

References

1. Lasaga, A. C., Soler, J. M., Gabor, J., Burch, T. E. & Nagy, K. L. Chemical weathering rate laws and global geochemical cycles. *Geochim. Cosmochim. Acta* **58**, 2361–2386 (1994).
2. Nugent, M. A., Brantley, S. L., Pantano, C. G. & Maurice, P. A. The influence of natural mineral coating on feldspar wheathering. *Nature* **395**, 588–591 (1998).
3. Kump, L., Brantley, S. L. & Arthur, M. A. Chemical weathering, atmospheric CO_2 and climate. *Earth Planet. Sci. Rev.* **28**, 611–667 (2000).
4. Scholze, H. Durability investigation of siliceous man-made mineral fibers: A critical review. *Glastechnische Berichte Glass Sci. Tech.* **61**, 161–171 (1988).
5. Filgueras, M. R., Latorre, G. & Hench, L. L. Solution effects on the surface reaction of bioactive glasses. *J. Biomed. Mater. Res.* **27**, 445–453 (1993).
6. Pisciella, P., Crisucci, S., Karamanov, A. & Pelino, M. Chemical durability of glasses obtained by vitrification of industrial wastes. *Waste Management* **21**, 1–9 (2001).
7. Hench, L. L. & Clark, D. E. Physical chemistry of glass surface. *J. Non-Cryst. Solids* **28**, 83–105 (1978).
8. Scholze, H. Glass water interactions. *J. Non-Cryst. Solids* **102**, 1–10 (1988).
9. Conradt, R. Chemical durability of oxide glasses in aqueous solutions: A review. *J. Am. Ceram. Soc.* **91**, 728–735 (2008).
10. Werme, L. O. *et al.* Chemical corrosion of highly radioactive borosilicate nuclear waste glass under simulated repository conditions. *J. Mater. Res.* **5**, 1130–1146 (1990).
11. Abraitis, P. K. *et al.* The kinetics and mechanisms of simulated British Magnox waste glass dissolution as a function of pH, silicic acid activity, and time in low temperature aqueous systems. *Appl. Geochem.* **15**, 1399–1416 (2000).
12. Pierce, E. M. *et al.* Accelerated weathering of a high-level and pu-bearing lanthanide borosilicate waste glass in a can-in-canister configuration. *Appl. Geochem.* **22**, 1841–1859 (2007).
13. Ewing, R. C. in *Scientific Basis for Nuclear Waste Management* Vol. 1 (ed. McCarthy, J. M.) 57–68 (1978).
14. Lutze, W., Malow, G., Ewing, R. C., Jercinovic, M. J. & Keil, K. Alteration of basalt glasses: Implications for modelling the long-term stability of nuclear waste glasses. *Nature* **314**, 252–255 (1985).
15. Casey, W. H. & Bunker, B. C. Mineral-water interface geochemistry. *Rev. Mineral.* **23**, 397–426 (1990).
16. Bunker, B. C. Molecular mechanisms for corrosion of silica and silicate glasses. *J. Non-Cryst. Solids* **179**, 300–308 (1994).
17. Alekseyev, V. A., Medvedeva, L. S., Prisyagina, N. I., Meshalkin, S. S. & Balabin, A. I. Change in the dissolution rates of alkali feldspars as a result of secondary mineral precipitation and approach to equilibrium. *Geochim. Cosmochim. Acta* **61**, 1125–1142 (1997).
18. Abraitis, P. K., McGrail, B. P., Trivedi, D. P., Livens, F. R. & Vaughan, D. J. Single-pass flow-trough experiments on a simulated waste in alkaline media at 40 °C. *J. Nucl. Mater.* **280**, 196–205 (2000).
19. Grambow, B. & Muller, R. First-order dissolution rate law and the role of surface layers in glass performance assessment. *J. Nucl. Mater.* **298**, 112–124 (2001).
20. Casey, W. H., Westrich, H. R., Banfiled, J. F., Ferruzzi, G. & Arnold, G. W. Leaching and reconstruction at the surfaces of dissolving chain-silicate minerals. *Nature* **366**, 253–256 (1993).
21. Tsomaia, N., Brantley, S. L., Hamilton, J. P., Pantano, C. G. & Mueller, K. T. NMR evidence for formation of octahedral and tetrahedral Al and repolymerisation of Si network during dissolution of aluminosilicate glass and crystal. *Am. Mineral.* **88**, 54–67 (2003).
22. Grambow, B. *Uhlig's Corrosion Handbook* 2nd edn 411–437 (Wiley, 2000).
23. Barkatt, A., Macedo, P. B., Gibson, B. C. & Montrose, C. J. Modelling of waste performance and system release. *Mater. Res. Soc. Symp. Proc.* **44**, 3–13 (1985).
24. Delage, F., Ghaleb, D. & Dussossoy, J. L. A mechanistic model for understanding nuclear waste glass dissolution. *J. Nucl. Mater.* **190**, 191–197 (1992).
25. Xing, S. B., Buechele, A. C. & Pegg, I. L. Effect of surface layers on the dissolution of nuclear waste glasses. *Mater. Res. Soc. Symp. Proc* **333**, 541–548 (1994).
26. Gin, S., Ribet, I. & Couillard, M. Role and properties of the gel formed during nuclear glass alteration: Importance of gel formation conditions. *J. Nucl. Mater.* **298**, 1–10 (2001).
27. Chick, L. A. & Pederson, L. R. The relationship between layer thickness and leach rate for nuclear waste glasses. *Mater. Res. Soc. Symp. Proc.* **26**, 635–642 (1984).
28. McGrail, B. P., Icenhower, J. P. & Cordova, E. A. Origins of discrepancies between kinetic rate law theory and experiments in the Na_2O–B_2O_3–SiO_2 system. *Mater. Res. Soc. Symp. Proc.* **713**, 537–546 (2002).
29. Hodson, M. E. The influence of Fe-rich coatings on the dissolution of anorthite at pH 2.6. *Geochim. Cosmochim. Acta* **67**, 3355–3363 (2003).
30. Advocat, T., Jollivet, P., Crovisier, J. L. & Del Nero, M. Long-term alteration mechanisms in water for SON68 radioactive borosilicate glass. *J. Nucl. Mater.* **298**, 55–62 (2001).
31. Scheetz, B. E. *et al.* The role of boron in monitoring the leaching of borosilicate glass waste forms. *Mater. Res. Soc. Symp. Proc.* **44**, 129–134 (1985).
32. Galoisy, L., Pelegrin, E., Arrio, M. A., Ildefonse, P. & Calas, G. Evidence for 6-coordinated zirconium in inactive nuclear waste glasses. *J. Am. Ceram. Soc* **82**, 2219–2224 (1999).
33. Angeli, F., Gaillard, M., Charpentier, T. & Jollivet, P. Influence of zirconium on the structure of pristine and leached soda-lime borosilicate glasses: Towards a quantitative approach by ^{17}O MQMAS NMR. *J. Non-Cryst. Solids* **354**, 3713–3722 (2008).
34. Porod, G. in *Small Angle X-ray Scattering* (eds Glatter, O. & Kratky, O.) 17–52 (Academic, 1982).
35. Brunauer, S., Emmett, P. H. & Teller, E. Adsorption of gases in multilmolecular layers. *J. Am. Chem. Soc* **60**, 309–319 (1938).
36. Calo, J. M. & Hall, P. J. The applications of small angle scattering techniques to porosity characteristics in carbons. *Carbon* **42**, 1299–1304 (2004).
37. Devreux, F., Ledieu, A., Barboux, P. & Minet, Y. Leaching of borosilicate glasses. II. Model and Monte Carlo simulations. *J. Non-Cryst. Solids* **343**, 13–25 (2004).
38. Ledieu, A., Devreux, F., Barboux, P., Sicard, L. & Spalla, O. Leaching of borosilicate glasses. I. Experiments. *J. Non-Cryst. Solids* **343**, 3–12 (2004).
39. Bourcier, W. L., Pfeiffer, D. W., Knauss, K. G., McKeegan, K. D. & Smith, D. K. A kinetic model for borosilicate glass dissolution affinity of a surface alteration layer. In scientific basis for nuclear waste management. *Mater. Res. Soc. Symp. Proc.* **176**, 209–216 (1990).
40. Grambow, B. A general rate equation for nuclear waste glass corrosion. *Mater. Res. Soc. Symp. Proc.* **44**, 15–27 (1985).
41. Linard, Y., Advocat, T., Jégou, C. & Richet, P. Thermochemistry of nuclear glasses: Application to weathering studies. *J. Non-Cryst. Solids* **289**, 135–143 (2001).
42. Gin, S., Jégou, C., Frugier, P. & Minet, Y. Theoretical consideration on the application of the Aagaard-Helgeson rate law to the dissolution of silicate minerals and glasses. *Chem. Geol.* **255**, 14–24 (2008).
43. Chave, T., Frugier, P., Ayral, A. & Gin, S. Solid state diffusion during nuclear glass residual alteration in solution. *J. Nucl. Mater.* **362**, 466–473 (2007).
44. Ferrand, K., Abdelouas, A. & Grambow, B. Water diffusion in the simulated French nuclear waste SON 68 contacting silica rich solutions: Experimental and modeling. *J. Nucl. Mater.* **355**, 54–67 (2006).
45. Liu, Y. C., Wang, Q. & Lu, L. H. Water confined in nanopores: Its molecular distribution and diffusion at lower density. *Chem. Phys. Lett.* **381**, 210–215 (2003).
46. Crovisier, J. L., Advocat, T. & Dussossoy, J. L. Nature and role of natural alteration gels formed on the surface of ancient volcanic glasses (Natural analogs of waste containment glasses). *J. Nucl. Mater.* **321**, 91–109 (2003).
47. Casey, H. W., Westrich, H. R., Arnold, G. W. & Banfield, J. F. The surface chemistry of dissolving labradorite feldspar. *Geochim. Cosmochim. Acta* **53**, 821–832 (1989).
48. Aagaard, P. & Helgeson, H. C. Thermodynamic and kinetic constraints on reaction rates among minerals and aqueous solutions. I. Theoretical considerations. *Am. J. Sci.* **282**, 237–285 (1982).
49. Lasaga, A. C. Fundamental approaches in describing mineral dissolution and precipitation rates. *Rev. Mineral.* **31**, 23–86 (1995).
50. Oelkers, E. H. General kinetic description of multioxide silicate mineral and glass dissolution. *Geochim. Cosmochim. Acta* **65**, 3703–3719 (2001).

Supplementary Information accompanies the paper at www.nature.com/naturematerials.

Acknowledgements

We acknowledge the help of Wahib Saikaly at CP2M (Marseille, France) for the scanning transmission electron microscopy experiments and the assistance of Laurent Dupuy at BiophyResearch (Marseille, France) for the ToF-SIMS experiments.

Author information

Reprints and permissions information is available online at http://npg.nature.com/reprintsandpermissions. Correspondence and requests for materials should be addressed to F.D.